Atomic transport processes on electrodes in liquid environment

2001 J. Phys.: Condens. Matter 13 5009

(http://iopscience.iop.org/0953-8984/13/21/325)

INSTITUTE OF PHYSICS PUBLISHING JOURNAL OF PHYSICS: CONDENSED MATTER

J. Phys.: Condens. Matter **13** (2001) 5009–5026 www.iop.org/Journals/cm PII: S0953-8984(01)18742-4

Atomic transport processes on electrodes in liquid environment

Margret Giesen[1] **and Sascha Baier**

Institut für Schichten und Grenzflächen, Forschungszentrum Jülich, 52425 Jülich, Germany

E-mail: m.giesen@fz-juelich.de

Received 8 November 2000

Abstract

We present an overview on the method of analysing equilibrium step fluctuations on metal electrodes to study atomic transport processes at the solid/liquid interface. It is demonstrated that this method provides an access road to a quantitative understanding of surface mobility on metal electrodes. Likewise it is shown that the investigation of step fluctuations is a method to determine activation energies and—with the help of recently introduced temperature dependence experiments—pre-exponential factors. We will show that the dependence of surface mobility on electrode potential and on the electrolyte may be rather complex. As examples, we present STM studies on stepped Cu(111) and Ag(111) electrodes in aqueous electrolytes. For Cu(111) in HCl, we find that the time dependence of step fluctuations obeys a $t^{1/3}$-law, which entails that step fluctuations are dominated by fast attachment/detachment kinetics at steps and slow terrace diffusion. For Ag(111) in $CuSO_4$ and H_2SO_4, an $L^{1/2}t^{1/2}$-dependence (with L the step distance) near the potential of fast Ag dissolution is observed. This time dependence corresponds to an atomic transport based on terrace diffusion and transport through the liquid. We also show that the results of temperature dependent studies of step fluctuations on Ag(111) are in excellent agreement with previous investigations concerning the potential dependence.

1. Introduction

Classic quantitative electrochemical measurements, e.g. current–potential or coulometric studies, are not capable of investigating the details of atomic transport on electrode surfaces in contact with a liquid. This is due to the fact that classic electrochemical studies integrate over the entire surface. Hence, differences in atomic transport on flat terraces on the one hand and at defects as steps, islands and kinks on the other hand are not considered. As has been demonstrated in studies on metal surfaces in UHV in recent years (for an overview see e.g. [1]), however, atomic mobility and mass transport may considerably be influenced by the presence of defects. With the development of electrochemical scanning tunnelling microscopes (EC-STMs) [2, 3] experimentalists have been provided with an experimental technique which

[1] Corresponding author. http://www.fz-juelich.de/igv/GIESEN/ag-giesen1.htm

0953-8984/01/215009+18$30.00

is capable of delivering direct information on the local surface structure, however, since mass transport on solid surfaces may be fast compared to the scanning speed, not necessarily on the local mass transport phenomena. During the last decade, studies in UHV showed that indirect, statistical methods may be used to analyse atomic motion on surfaces quantitatively [1]. From step correlation functions [4–8], e.g. one may determine the dominant mass transport mechanism which causes steps on surfaces to fluctuate in equilibrium [9–24]. Temperature variable studies may then also provide information on the activation energies involved. These indirect statistical methods, however, require a large database to yield results with sufficient accuracy. It was shown that an excellent database for surfaces in UHV requires the recording of several hundred of STM images [1–3]. While it requires already painstaking work to achieve statistical relevant results in UHV, it seems to be even harder to obtain a sufficient database for surfaces in electrolyte: first, because extended measurements to obtain enough data over a long time are difficult; second, because remaining thermal drift in the electrolyte prevent measurements in the same surface area; third, because temperature dependent studies may be rather toilsome due to the influence of thermal drift as well as to a relatively small temperature range available. Furthermore, for surfaces in electrolyte the electrode potential as well as the electrolyte may have a considerable influence on the surface mobility and must therefore be considered. Due to these difficulties and due to the lack of other methods providing local and quantitative information, the knowledge of the surface mobility on electrodes in electrolyte have so far mostly been merely a qualitative one.

It is only very recently that we have begun to apply the aforementioned statistical concepts to surfaces in liquid environment. Despite some studies on island ripening [25, 26] most effort has been spent, in particular, on the quantitative analysis on equilibrium step fluctuations on metal electrodes in electrolyte [27–32]. The investigations available so far indicate that quantitative studies of step fluctuations on metal electrodes are worth the effort: by studying equilibrium step fluctuations, dominant atomic mass transport mechanisms at a given electrode potential were identified and transport related activation energies were estimated [27, 29, 32]. Direct access to these energies, however, would be provided by temperature dependent studies of the surface mobility. Although such studies in liquid environment have been widely neglected so far, we could prove very recently that activation energies and pre-exponential factors are measurable even for aqueous electrolytes where merely a small temperature range is accessible [30].

In this report, we will give an overview of the method of analysing equilibrium step fluctuations at the solid/liquid interface. We will focus our presentation, in particular, on temperature dependent investigations. The results obtained from these temperature variable studies will be compared to the estimated activation energies provided by the previous potential dependent investigations at room temperature. We also compare the results measured at the solid/liquid interface with those determined in UHV. It is demonstrated that despite some similarities characteristic differences have to be considered. The paper is organized as follows. In the next section, we provide the reader with a description of the experimental set-up and of the preparation of the metal electrodes as well as of the specific appearance of mobile steps in STM images. In section 3, we present a review of the theoretical aspects on the analysis of step fluctuations. Section 4 is devoted to the experimental results to be discussed in section 5.

2. Experiment

2.1. Temperature variable electrochemical STM

Our temperature variable electrochemical scanning tunnelling microscope (EC-STM) is based on the electrochemical version of a Topometrix TMX 2010 Discoverer STM, which

independently controls the tip and sample potential via a bipotentiostat. In the STM version of this instrument, a metal socket is used as a sample stage, which is replaced by the scanner in the atomic force microscope (AFM) version. In the STM version, however, the sample stage has no further technical relevance other than to guarantee the same general scanner–sample geometry and to provide for an easy exchange between STM and AFM application. Therefore, we replaced the metal socket by a home-built heating and cooling stage containing a Peltier element [30]. Figure 1(a) shows a schematic sketch of our temperature variable STM set-up during tunnelling. The Peltier element is placed at the bottom of a copper block. The latter may be either heated or cooled depending on the direction of the applied current to the Peltier element. At the top of the copper block small magnets as well as a thermo-resistance are integrated. The former serve as a supply for the electrochemical cell, which has a nickel bottom. The electrochemical cell is in direct thermal contact with the thermo-resistance and the temperature T_0 is measured at the back of the cell. T_0 is regulated by an analogue control loop. Due to thermal loss across the bottom of the electrochemical cell and the sample, the temperature at the sample surface T_S deviates slightly, but linearly, from T_0 (figure 1(b)). Therefore, the surface temperature may be easily calibrated during experiment when the sample is in thermal equilibrium. As can be seen from the inset of figure 1(b), an off-set in the sample temperature T_S of 2.25 °C for $T_0 = 0$ °C is measured. When T_0 is changed by several degrees, thermal equilibrium of the electrode is established within a few minutes. Then, the thermal drift of the microscope is smaller than 50 Å min^{-1}.

The maximum and minimum temperatures that can be reached at the surface are limited by convection in the electrolyte causing a strong drift during the scanning process and by the freezing point of the electrolyte, respectively. The maximum temperature is furthermore restricted by the increased evaporation rate of the electrolyte at elected temperatures which also causes a shift in electrode potential due to the change in electrolyte concentration. Hence, reliable experiments in aqueous electrolytes are possible in a temperature range between 5 and 50 °C.

2.2. Sample preparation and electrolytes

The quantitative analysis of equilibrium step fluctuations requires a large data set. Therefore, it is recommended to use vicinal surfaces with regular step arrays of parallel, equidistant steps along the atomically dense direction ($\langle 110 \rangle$ in the case of fcc metals as used in our studies). These surfaces have the further advantage that possible step pinning, which causes geometrical kinks into the step edge, is reduced to a minimum. As we will see in section 3, geometrical kinks may introduce substantial error into the analysis.

The stepped electrodes were cut by spark erosion from a single crystal rod, oriented by diffractometry and polished to the desired orientation to within 0.1°, which is the accuracy of high quality single crystals. The accuracy is naturally limited by the mosaic structure of the crystal.

2.2.1. Stepped Cu(111) electrodes. The stepped Cu(111) electrodes had a nominal orientation of (39, 39, 37) (corresponding to a miscut of 1.4° about the $\langle \bar{2}11 \rangle$-direction). This surface consists of 90 Å wide (111)-terraces separated by so-called B-steps. These steps form a (111)-oriented micro-facet with the underlying terrace. To decrease the sulphur content of the copper crystals, the samples were heated for several hours in an H:Ar (1:25) atmosphere at 800 °C. Prior to experiment, the Cu electrodes were electropolished in 66% ortho-phosphoric acid at 2.2 V for 15 s in the electrochemical STM cell. After thoroughly rinsing the cell and the electrode surface with deaerated Milli-Q water (18.2 MΩ cm^{-1}), the surface was protected

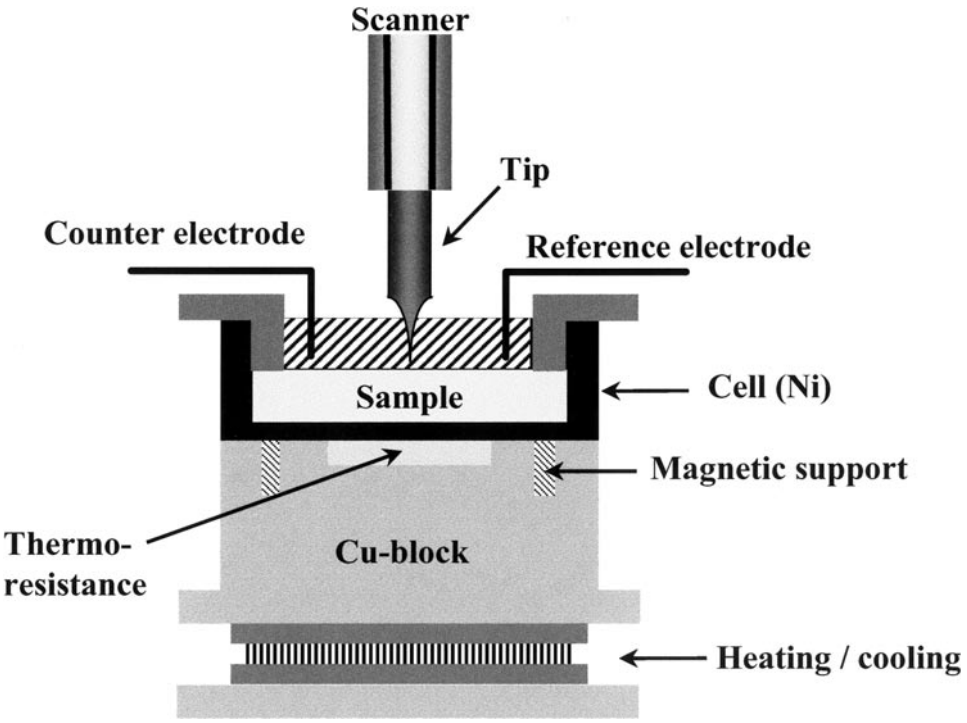

(a)

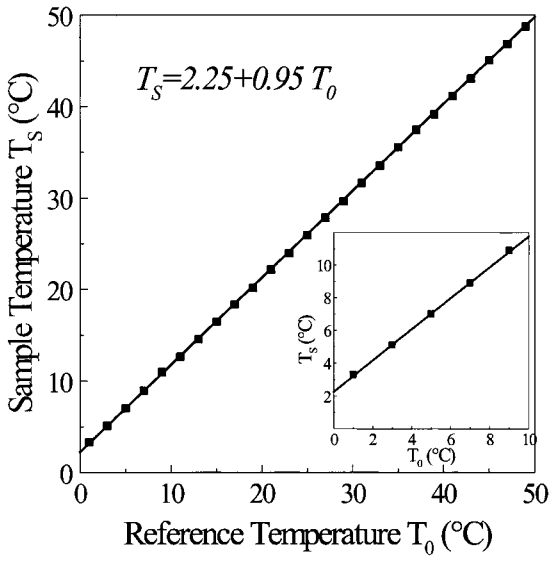

(b)

Figure 1. (a) Schematic sketch of the temperature variable STM used in our studies. (b) Temperature calibration of the surface temperature T_s for a given temperature T_0 at the thermo-resistance. The inset shows a close-up of the same data at low temperatures.

against oxidation by a drop of electrolyte which was degassed by purging with oxygen-free argon. Subsequently, the electrochemical STM cell was connected to the bipotentiostat.

The tunnelling tips were etched from polycrystalline tungsten wires and coated with polyethylene to avoid Faraday currents at the foremost part of the tip [33]. In all experiments, the tunnelling current was 2 nA. For the potential dependent measurements, the tunnelling bias varied between +100 and +450 mV, while for the temperature variable studies the bias was held constant at +400 mV. High purity, flame-annealed Pt wires (Goodfellow, 99.999%) served as counter and quasi-reference electrodes. In the following, the electrode potentials of the metal samples are, however, given with respect to the saturated calomel electrode (SCE). As an electrolyte, we used suprapure HCl (Merck) and Milli-Q water (Millipore, 18.2 MΩ cm^{-1}).

2.2.2. Stepped Ag(111) electrodes. The experiments on the stepped Ag(111) electrode were performed on nominally (19, 19, 17)- and (33, 33, 31)-oriented crystals (corresponding to a miscut of 2.9°, respectively, 1.7° about the $\langle\bar{2}11\rangle$-direction). These surfaces consist of 46 Å, respectively 81 Å, wide (111)-terraces separated by atomically dense B-steps. Prior to experiment, the Ag crystals were chemically prepared in H_2O_2/cyanide and H_2O_2 solutions and subsequently flame annealed while the surface was kept in a flowing argon atmosphere.

The tunnelling tips were etched in a cyanide solution from a Pt/Ir (80:20) wire and coated with an electrophoretic paint (BASF Glasophor) by means of galvanostatic deposition, leaving only the foremost part of the tunnelling tip exposed to the electrolyte [33]. The tunnelling current was 2 nA. For the potential dependent measurements, the tunnelling bias was varied between +40 and +80 mV, while for the temperature-variable experiments the bias was kept at +50 mV. As an electrolyte, we used 1 mM $CuSO_4$ + 0.05 M H_2SO_4, which was made from suprapure (H_2SO_4) and p.a. ($CuSO_4$) chemicals (Merck) and Milli-Q water (Milipore, 18.2 MΩ cm^{-1}). Copper and platinum wires of high purity (Goodfellow, 99.999%) served as a reference and counter electrode, respectively.

Both the Cu as well as the Ag electrodes were re-orientated and re-polished after approximately ten individual experiments.

2.3. Frizzy appearance of mobile steps in STM images

Mobile steps on surfaces reveal a certain roughness when displayed in STM images, which is called 'step frizziness'. Frizzy steps were first observed on metal surfaces in UHV [34] and interpreted as kink motion along steps rather than be attributed to tip noise [35, 36]. The step frizziness manifests itself in sudden jumps in the step position caused by kinks crossing the scan line during the scanning process. If the kink mobility at steps is low, the step position is found at lattice positions, as is observed, e.g. for Cu(100) in UHV below 320 K [14]. If the kink mobility is high, the step position may be found at non-integer multiples of the distance between equivalent lattice positions (see also, e.g. stepped Cu(100) surfaces in UHV at 500 K [12]). Due to the kink motion during the scanning process, STM images of frizzy steps are not exclusively spatial images, but include time information. The pure time information can be extracted by the use of so-called time images (sometimes denoted as x–t-scans) [37]. In time images, a single scan line is recorded repetitively and subsequent scan lines are then displayed in pseudo-images where one axis is a time and the other is a spatial axis.

Frizzy steps are also observed in STM images of metal electrodes in liquid environment. Dietterle *et al* were the first to report frizzy steps on Ag(111) electrodes in electrolyte [38]. Meanwhile, frizzy steps have been observed on several metal electrodes [26, 29–32, 39]. Figure 2 shows time images of (a) the stepped Cu(111) surface at $T = 300$ K and $U = -420$ mV against the SCE and (b) the stepped Ag(111) surface at $T = 296$ K and $U = +50$ mV against the SCE. In the images displayed in figure 2, the time axis is oriented

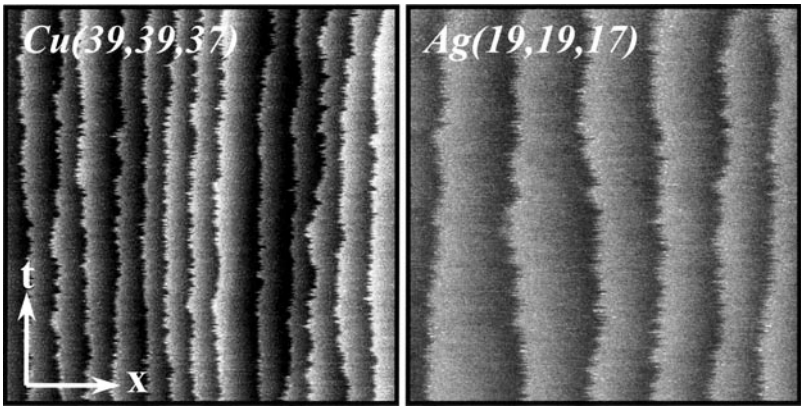

Figure 2. Time images of Cu(39, 39, 37) in 1 mM HCl at $T = 300$ K, $U = -420$ mV against the SCE and Ag(19, 19, 17) in 1 mM $CuSO_4$ + 0.05 mM H_2SO_4 at $T = 296$ K, $U = +50$ mV against the SCE. The scan widths (normal to the steps) in the images are 130 and 40 nm, respectively. The total time displayed on the t-axis (parallel to the steps) is 40 and 21 s, respectively.

from bottom to top (approximately parallel to the step edges) and the spatial axis from left to right (approximately perpendicular to the steps).

As a caveat it is finally mentioned that spatial information may be extracted from normal STM images only if steps do not appear frizzy! This circumstance is particular important, if one wants to extract quantitative spatial information from STM studies of mobile steps as will be discussed in the following.

3. Theory

Step fluctuations are conveniently analysed by means of a step correlation function $G(y, t)$, which is defined as the mean square deviation of step positions x in different scan lines y, y_0 and at different times t, t_0:

$$G(y, t) = \langle (x(y, t) - x(y_0, t_0))^2 \rangle. \tag{1}$$

The Cartesian coordinates are defined such that x and y are the coordinates perpendicular and parallel to the average step orientation, respectively[2]. Without restriction of generality, the reference values y_0, t_0 are set to zero in the following.

3.1. Spatial correlation function $G(y)$

In the limit of low kink mobility, STM images represent snap shot images of the surface and the time dependence of the correlation function can be neglected:

$$G(y) = \langle (x(y) - x(0))^2 \rangle. \tag{2}$$

In experiment, the kink mobility can be expected to be low in the limit of low temperatures (e.g. for Cu(100) in UHV below 300 K [14, 16]). For metal electrodes in electrolyte, the kink mobility is further influenced by the electrode potential. In the studies performed so far, the kink mobility was low in the limit of cathodic potentials. $G(y)$ could be interpreted as merely spatial, however, only in the case of Au(111) in sulphuric and chloric acid [32].

[2] This notation is frequently referred to as 'Maryland notation' since it was introduced by the group at the University of Maryland, College Park [40] and is now used by many experimentalists and theorists.

For uncorrelated kink motion, $G(y)$ is a linear function of the distance y [40]:

$$G(y) = \langle (x(y) - x(0))^2 \rangle = \frac{b^2(\theta, T)}{a_\parallel} |y|. \tag{3}$$

Here, $a_\parallel$ is the nearest-neighbour distance along the atomically dense direction which is $\langle 110 \rangle$ for fcc metals. The diffusivity b^2 depends on temperature and on the angle θ between the atomically dense $\langle 110 \rangle$-direction and the average orientation of the steps. For densely packed steps ($\theta = 0$) and not too high temperatures, where kinks are of monatomic length, the diffusivity can be written in terms of the kink formation energy ε:

$$b^2(\theta = 0, T) = \frac{2a_\perp^2}{2 + \mathrm{e}^{\varepsilon / k_B T}}. \tag{4}$$

Here, $a_\perp$ is the distance between adjacent atomically dense rows[3]. If $k_B T \ll \varepsilon$, equation (4) reduces to

$$b^2(\theta = 0, T) \approx 2\,\mathrm{e}^{-\varepsilon / k_B T} a_\perp^2 = P_k a_\perp^2 \tag{5}$$

with P_k the kink concentration. Assuming only nearest-neighbour interactions, b^2 can be expressed for steps off the atomically dense direction (e.g. pinned steps or steps on vicinal surfaces with non-zero azimuthal miscut angle), by [41–43]

$$\frac{b^2(\theta \neq 0, T)}{a_\perp^2} = \tan^2 \theta + \frac{4z^2 + (1 + z^2)\sqrt{4z^2 + (1 - z^2)^2 \tan^2 \theta}}{(1 - z^2)^2} \tag{6}$$

with $z = \mathrm{e}^{-\varepsilon / k_B T}$.

Recently, we have shown [44] that experimental results on stepped Cu(100) surfaces with polar as well as azimuthal misorientation with respect to $\langle 110 \rangle$ are better described by

$$b^2(\theta \neq 0, T) = \frac{r''(\xi) r(\xi)}{\left(1 + [r'(\xi)]^2\right)^{3/2}} \frac{k_B T}{\gamma(0)} \bigg|_{\xi = 0}. \tag{7}$$

Here, $r(\xi)$ is the contour line of the equilibrium shape of an island and $\xi = 0$ denotes the coordinate at the quasi-straight segment of the island perimeter, i.e. $r(\xi)$ represents a point in the middle between two rounded island corners[4]. $r'(\xi = 0)$ and $r''(\xi)$ denote the first and the second derivative of the contour $r(\xi)$ with respect to ξ. The step energy per atom $\gamma(0)$ is taken at $r(\xi = 0)$ and may be approximated by $\gamma(0) \approx \varepsilon$ and $\approx 2\varepsilon$ [46] for square and hexagonal lattices, respectively.

From equations (3) and (5), one finds that the kink concentration and the kink formation energy may be determined from an analysis of the spatial correlation function $G(y)$ of parallel, densely packed steps (i.e. $\theta = 0$). For Au(111) in 0.1 M H_2SO_4 + 0.5 mM HCl, e.g. the kink energy was measured as 74 meV at −100 mV against the SCE using this method [32]. We emphasize that for $\theta \neq 0$, $b^2(\theta \neq 0, T)$ is larger than $b^2(\theta = 0, T)$ at a given T according to equations (6) and (7). Hence, if pinned steps were analysed using equation (5) the determined value for ε would be too low.

Finally, it is emphasized that the time information is dominant in STM images if steps are frizzy. Then, the coordinate y is in fact a time axis. While $G(y, t)$ is linear in y (equation (3)) the dependence of $G(y, t)$ on the time is a power law with an exponent smaller than 1 (as discussed in the next section). Therefore, the slope determined from a linear fit to $G(y, t)$ in the case of frizzy steps is not related to the kink concentration.

[3] For fcc (100)-surfaces, $a_\parallel = a_\perp = a_0/\sqrt{2}$, a_0 being the lattice constant. For fcc (111)-surfaces, $a_\perp = a_0\sqrt{3}/(2\sqrt{2})$.

[4] The two-dimensional equilibrium shape of islands reveals no facets since steps are above the roughening transition [45] for $T > 0$ K. Hence, island edges are never straight but slightly curved. For low temperatures, however, the curvature of particular island segments may be small such that these island segments are quasi-straight and oriented approximately along a dense atomic direction [46].

3.2. Time correlation function $G(t)$

In the limit of high kink mobility (this case applies, e.g. for Cu(111) and Ag(111) in UHV already at room temperature [1, 12]), STM images reveal exclusively time information and the spatial contribution to $G(y, t)$ can be neglected:

$$G(t) = \langle (x(t) - x(0))^2 \rangle. \tag{8}$$

According to theory [4–8], $G(t)$ obeys different time laws, depending on the mass transport mechanism mediating the step fluctuations:

$$G(t) = c(T, U) L^{\delta} t^{\alpha}. \tag{9}$$

Here, $c(T, U)$ is a temperature and potential dependent pre-factor and L is the step–step distance. The exponents δ and α depend on the dominant mass transport mechanism and may assume values $\delta = 0, +1/4, \pm 1/2$ and $\alpha = 1/4, 1/3, 1/2$. A specific combination of values is unique for a particular mass transport situation. That is, if one measures the exponents α and δ, the dominant mass transport mechanism on the surface is determined. An overview over all mass transport cases and the related time laws serving to the needs of an experimentalist is given in [1, 27]. Here, we restrict ourselves to few cases needed for the analysis of the experimental data presented in this paper.

3.2.1. Case of atomic diffusion alongside step edges. If the mass transport is restricted to the step edges, the time dependence of $G(t)$ is [4]

$$\frac{G(t)}{a_{\perp}^2} \approx 0.464\, P_k^{3/4} D_{st}^{1/4} t^{1/4}. \tag{10}$$

Here, P_k is the kink concentration as before and D_{st} is the chemical mass diffusion coefficient along a kinked step. In the case of one diffusing mass species and low species concentration c_{st}, D_{st} can be expressed in terms of the tracer diffusion coefficient D_{st}^{tr} : $D_{st} = c_{st} D_{st}^{tr}$. Assuming the chemical mass diffusion coefficient D_{st} to be an activated quantity with pre-exponential factor we rewrite:

$$D_{st} = \nu\, \mathrm{e}^{-E_{st}/k_B T}. \tag{11}$$

Using equations (5) and (11), equation (10) becomes (with $4E = 3\varepsilon + E_{st}$)

$$\frac{G(t)}{a_{\perp}^2} \approx 0.78\, \nu^{1/4}\, \mathrm{e}^{-E/k_B T} t^{1/4}. \tag{12}$$

In equations (10)–(12), as in the following, diffusion coefficients as well as kink and adatom concentrations are given in atomic units, i.e. the kink and adatom concentration are given as kinks, respectively adatoms, per atom and diffusion coefficients have units s^{-1}. Furthermore, the energy E denotes the activation energy determined from an Arrhenius plot of measured data of $G(t)$ in equation (12) and in the following. Depending on the dominant mass transport, the energy E may be differently related to the kink and diffusion energies.

Another mass transport situation where the time exponent α is $1/4$ is the case of exchange atoms between neighbouring steps in the presence of a large Ehrlich–Schwoebel barrier [47, 48], which is an additional activation barrier for crossing of steps. In this case, however, $G(t)$ depends also on the step–step distance L with $\delta = 1/4$.

3.2.2. Case of atomic exchange between steps and terrace with slow terrace diffusion. Here, atoms detach from isolated steps onto the terrace and the diffusion on the terrace is slow compared to the detachment process. Then, $G(t)$ is given by [5]

$$\frac{G(t)}{a_\perp^2} \approx 1.086\, P_k^{2/3} D_t^{1/3} t^{1/3}. \tag{13}$$

D_t is the chemical mass diffusion coefficient on the terrace and may be expressed for one diffusing species and for low species concentration c_t as $D_t = c_t D_t^{tr}$. Here, D_t^{tr} is the tracer diffusion coefficient on the terrace. Again, we rewrite D_t as an activated quantity:

$$D_t = \nu\, \mathrm{e}^{-E_t/k_B T}. \tag{14}$$

Then, equation (13) becomes (now choosing $3E = 2\varepsilon + E_t$)

$$\frac{G(t)}{a_\perp^2} \approx 1.587\, \nu^{1/3}\, \mathrm{e}^{-E/k_B T} t^{1/3}. \tag{15}$$

So far, the case in equation (15) has been studied only in theoretical investigations using Monte Carlo simulations [4]. It was not observed in any of the experimental studies in UHV. As will be shown in the next section, for Cu(111) in electrolyte we were able to demonstrate for the first time that this mass transport situation may be realized in an electrochemical environment.

3.2.3. Case of atomic exchange between steps and terrace with fast terrace diffusion. In this case, atoms are also exchanged between isolated steps and terraces; however, in contrast to the case before, terrace diffusion is fast compared to detachment of atoms from steps. Then, $G(t)$ is determined by the detachment rate and is given by [4, 36]

$$\frac{G(t)}{a_\perp^2} \approx \sqrt{\frac{2}{\pi}} P_k \nu_a^{1/2} t^{1/2} \tag{16}$$

where ν_a is the creation frequency of adatoms on terraces from kink sites. A $t^{1/2}$-dependence is also found in the next case where $G(t)$ depends also on the step–step distance L, however.

3.2.4. Exchange between neighbouring steps, terrace and the surrounding phase. While this case generally does not apply in UHV investigations where desorption is negligible, it is of particular importance for studies in electrolyte. Atoms are exchanged between steps and terraces and, after a mean diffusion path on the surface, may desorb (dissolve) into the adjacent phase which is the electrolyte in the liquid system. If the mean diffusion path is of the same order or even larger than the mean step–step distance (i.e. neighbouring steps may also serve as atom sinks and sources), $G(t)$ is given by [6–8]

$$\frac{G(t)}{a_\perp^2} \approx \left(P_k \frac{c_t}{\tau_{sl}} \right)^{1/2} L^{1/2} t^{1/2}. \tag{17}$$

Here, $c_t = \mathrm{e}^{-E_{ad}/k_B T}$ is the adatom concentration on the terrace with E_{ad} the adatom formation energy from kink sites. τ_{sl} is the mean time before surface atoms desorb into the adjacent phase (liquid) and can be written as

$$\tau_{sl} = \nu^{-1}\, \mathrm{e}^{E_{sl}/k_B T}. \tag{18}$$

Then, equation (17) becomes (for this case choosing $2E = \varepsilon + E_{ad} + E_{sl}$)

$$\frac{G(t)}{a_\perp^2} \approx \sqrt{2}\, \nu^{1/2}\, \mathrm{e}^{-E/k_B T} L^{1/2} t^{1/2}. \tag{19}$$

This mass transport situation is distinguished from all other cases with time exponent $\alpha = 1/2$ by the unique dependence of the time correlation function on the step–step distance L with exponent $\delta = +1/2$. If, e.g. the mean diffusion path is much smaller than the mean step–step distance, $G(t)$ is independent of L, and hence, $\delta = 0$, while α is still $1/2$. On the other hand, if atomic exchange into the adjacent phase is small and atoms dominantly exchange between neighbouring steps and terraces, $\delta = -1/2, \alpha = 1/2$. This case demonstrates, like no other, the sensitivity of $G(t)$ to the underlying dominant mass transport mechanism.

4. Experimental results

4.1. Stepped Cu(111) in chloric acid

The STM studies on Cu(111) were performed in 10 mM and 1 mM HCl solutions at 300 and 305 K, respectively. Figure 3(a) shows the correlation value $G(t_0)$ for $t_0 = 2$ s against the electrode potential for both electrolytes represented as circles and triangles, respectively. The data points are an average over about five individual measurements and determined from up to 100 steps. From the mean square deviation of the individual results one finds the error bars which have been plotted for both data sets. Within the scattering, the time correlation values show no systematic increase with the electrode potential. This is in contrast, e.g. with Ag(111) in 1 mM $CuSO_4$ + 0.05 mM H_2SO_4 [27] and Cu(100) in 5 mM H_2SO_4 [29] where $G(t_0)$ strongly increases with increasing electrode potential. For Cu(111) in 1 and 10 mM HCl, the fluctuations are independent of the potential between -500 mV and -150 mV against the SCE. In this potential range, chloride is specifically adsorbed on the Cu(111) surface but the ordered $(\sqrt{3} \times \sqrt{3})$R30° chloride structure [26, 49] is not necessarily yet formed: the formation of the superstructure is observed at different potentials for the two electrolytes. For a concentration of 1 mM HCl the formation of the ordered superstructure starts around -150 mV; for 10 mM HCl it starts around -250 mV. Therefore, the data points in figure 3(a) obtained at the highest potential were obtained while the surface was slowly restructuring.

In figure 3(b), $G(t)$ is plotted for different temperatures. The step fluctuations increase with increasing temperature. The time exponent is determined from least-squares fits to a power law in time which is demonstrated for $T = 298$ K in figure 3(c). The experimental data is represented by circles and the lines are fits with exponents $1/4$ (dotted), $1/2$ (dashed) and 1/3 (solid). The experimental data is obviously in agreement with a $t^{1/3}$-law. We find that the time dependence is best described by a time exponent $1/3$ for all temperatures between 296 and 307 K and for all electrode potentials between -500 and -150 mV against the SCE. According to equation (15), a time exponent $1/3$ is expected if the step fluctuations are dominated by a fast attachment/detachment kinetics at the step edges and slow terrace diffusion. For this case, $G(t)$ should be independent of the step–step distance L. We have checked this requirement and measured $G(t)$ for different values of L. The result shown in figure 3(d) is in accordance with equation (15).

We have measured the activation energy of the dominant mass transport mechanism. Figure 4 shows an Arrhenius plot of the time correlation value $G(t_0)$ for $t_0 = 1$ s in the temperature range between 289 and 305 K. From the mean slope, one finds an activation energy of

$$E_{Cu} = 0.28 \pm 0.04 \text{ eV} \tag{20}$$

where the subscript denotes that the activation energy was measured for Cu(111) and for further analysis equation (15) is used.

With equation (15), one obtains for the pre-exponential factor

$$\nu_{Cu} = 1.5 \times 10^{16\pm2} \text{ s}^{-1} \tag{21}$$

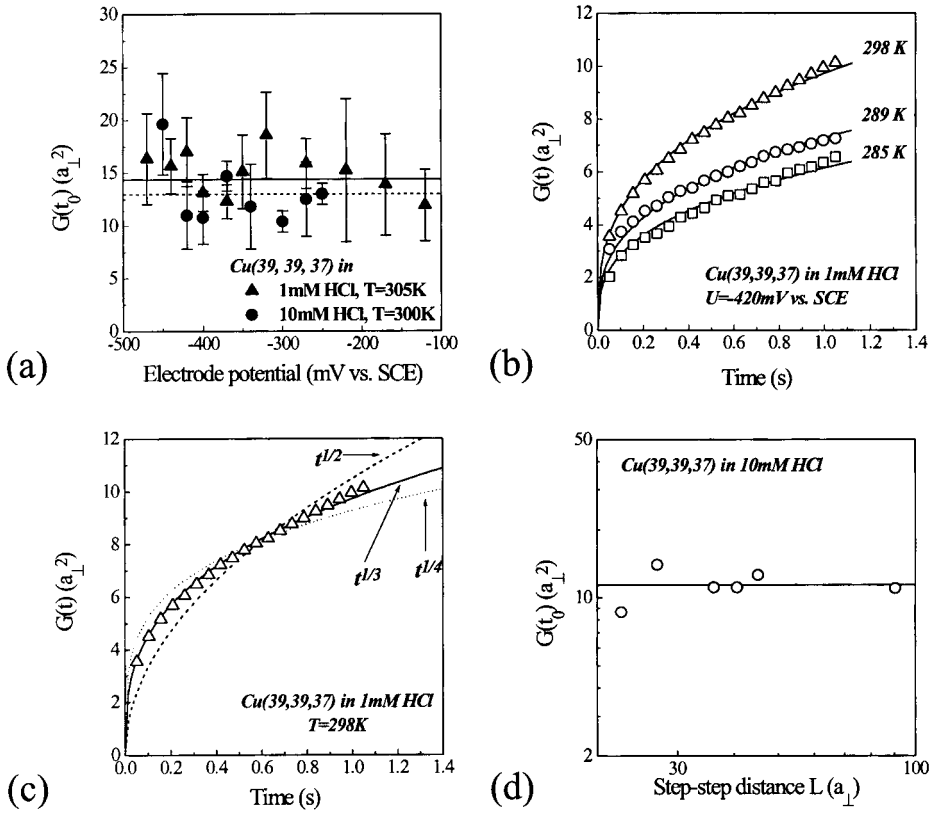

Figure 3. (a) Time correlation value $G(t_0)$ in 1 and 10 mM HCl for $t_0 = 2$ s and $T = 305$ K, respectively 300 K, against the electrode potential. The mean values of $G(t_0)$ are plotted as solid and dashed lines, respectively. (b) Time correlation function $G(t)$ for stepped Cu(111) in 1 mM HCl at $U = -420$ mV against the SCE for different temperatures. (c) Time correlation function $G(t)$ for stepped Cu(111) in 1 mM HCl for $T = 298$ K and $U = -420$ mV against the SCE. The lines are least-squares fits to power laws in time with exponents $1/4$ (dotted), $1/2$ (dashed) and $1/3$ (solid). (d) Log–log plot of the time correlation value $G(t_0)$ for $t_0 = 1$ s and -400 mV against the SCE measured on stepped Cu(111) in 10 mM HCl versus the step–step distance L.

which is considerably larger than what is typically found for metal surfaces in UHV ($\nu_0 \sim 10^{13}$ s^{-1} [50]).

4.2. Stepped Ag(111) in sulphuric acid

A detailed, exclusively *potential*-dependent study of equilibrium step fluctuations on stepped Ag(111) in 1 mM $CuSO_4$ + 0.05 M H_2SO_4 was reported several years ago [27]. It was shown that $G(t) \propto t^{1/4}$ (no L-dependence) for electrode potentials below 0 mV against SCE. For potentials above 0 mV against SCE, but still below the potential of rapid Ag dissolution, which is about +100 mV against SCE, $G(t) \propto L^{1/2}t^{1/2}$ was found. That is, for negative electrode potentials (with respect to the SCE), the step fluctuations are dominated by edge diffusion, while for positive electrode potentials, silver is exchanged between the electrode surface and the double layer of the electrolyte already before rapid Ag dissolution sets in. The change in the dominant mass transport mechanism around 0 mV is accompanied by a strong increase in the step fluctuations, which was demonstrated in the previous work by measuring the value

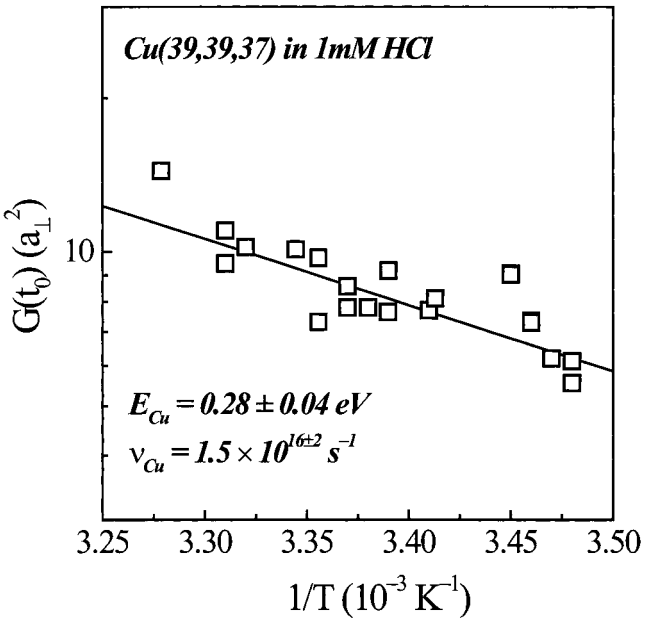

Figure 4. Arrhenius plot of the temperature dependent time correlation value $G(t_0)$ for stepped Cu(111) in 1 mM HCl at $t_0 = 1$ s and $U = -420$ mV against the SCE.

of $G(t)$ at a distinct reference time t_0 as a function of the electrode potential [27]. In it was shown that $G(t_0)$ is almost constant (within the error bars) for negative potentials and increases exponentially close to the dissolution potential.

To qualify our temperature-variable experimental STM set-up and our electrochemical system, we have first reproduced the previous measurements [27] of the time and potential dependence of the time correlation function at room temperature. Our new results are in agreement with the previous study; in particular, they confirm the step–step distance dependence of $G(t)$ in the positive potential range: figure 5(a) shows a log–log of $G(t_0)$ at $t_0 = 10$ s against the step–step distance L. The data is corrected for a constant off-set $G(0)$ of $G(t)$ at $t = 0$. This constant off-set, although not explained by theory and although never observed in UHV studies, seems to be characteristic for at least two systems in electrolyte studied so far: it was first observed for Ag(111) in 1 mM $CuSO_4$ + 0.05 M H_2SO_4 [27] and confirmed by our new measurements presented here. A $G(0)$ was also measured for Au(111) in 1 mM KI+50 mM $KClO_4$ by McHardy *et al* [31]. A constant off-set seems not to be generally present for metal electrodes in contact with a liquid, however. It was measured neither for Cu(111) in 1 and 10 mM HCl (as demonstrated in the last section) nor for Cu(100) in 0.05 M H_2SO_4 [29], and also not for Au(111) in 0.1 M H_2SO_4+ (0.01–50 mM) HCl [32]. The physical meaning of $G(0)$ is not understood yet. It was proposed that it may be due to tip–surface interactions, which, however, was not corroborated by experiment [29].

In figure 5(a), the circles represent the previously published data [27] and the squares are our new data. Both data sets agree, and when fitted to a straight line an average slope of $\delta = 0.59 \pm 0.14$ is determined. Figure 5(b) shows the time correlation value $G(t_0)$ for $t_0 = 11$ s corrected for the constant off-set at $G(0)$ against the electrode potential. Again, the circles are the previously obtained data [27] and the squares represent the new results. Obviously, the squares fall on the same strongly increasing curve. The temperature variable data discussed in

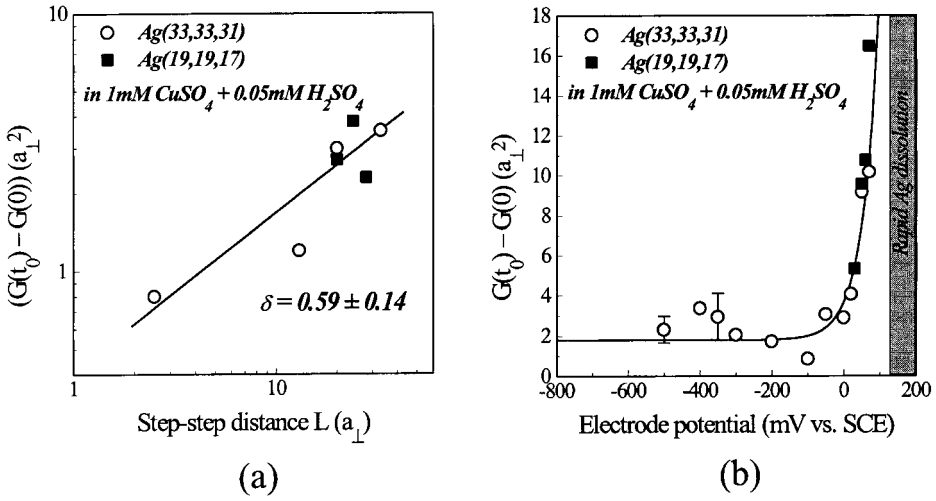

Figure 5. (a) Time correlation value $G(t_0)$ for $t_0 = 10$ s against the step–step distance L. (b) Time correlation value $G(t_0)$ for $t_0 = 11$ s against the electrode potential. The solid line is a fit to an exponential. In both graphs, the circles are the data taken from [27]; the squares represent our new results. Both data sets are corrected for the off-set of $G(t)$ for $t = 0$ and were obtained at $T = 300$ K (see text for discussion).

the following was obtained at a constant potential of +50 mV against SCE where the system is close to, but yet below the potential of rapid Ag dissolution (figure 5(b)).

Figure 6 shows the time correlation function $G(t)$ minus the constant off-set $G(0)$ as measured on stepped Ag(111) at an electrode potential of +50 mV against SCE for different temperatures. $G(t)$ increases with increasing temperature. For the determination of the corresponding activation energy to the correlation functions in figure 6, we have plotted the time correlation value $G(t_0)$ for $t_0 = 2$ s in an Arrhenius plot (figure 7). When fitted to a straight line the slope is

$$E_{Ag} = 0.55 \pm 0.10 \text{ eV} \tag{22}$$

where the subscript serves as a reminder that this activation energy was measured for Ag(111) and for further analysis equation (19) is used.

With equation (19), we determine the pre-exponential factor as

$$\nu_{Ag} = 3.4 \times 10^{16\pm3} \text{ s}^{-1}. \tag{23}$$

Similar to what is observed for Cu(111), the pre-exponential factor $3.4 \times 10^{16\pm3}$ s^{-1} found for Ag(111) in electrolyte is higher than the theoretical value in UHV (10^{13} s^{-1} [50]).

5. Discussion

5.1. Stepped Cu(111) in hydrochloric acid

Cu(111) in 1 mM HCl is the first experimental system, where the equilibrium step fluctuations are dominated by fast attachment/detachment kinetics and slow terrace diffusion. So far, the $t^{1/3}$-dependence was considered only in theoretical studies and simulations [5]. Here, we have demonstrated that this mass transport mechanism (although not observed in UHV studies to far) may be realized in liquid environment. The $t^{1/3}$-dependence of $G(t)$ for Cu(111) in hydrochloric acid is in qualitative agreement with recent experiments by Broekmann *et al*

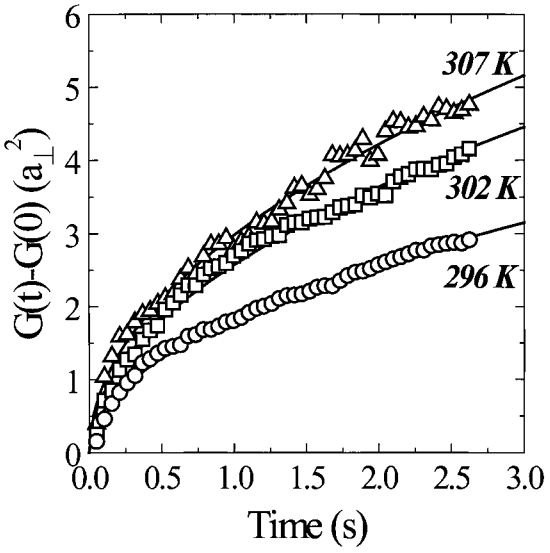

Figure 6. Time correlation function $G(t)$ reduced by the constant offset $G(0)$ at $t = 0$ as measured for stepped Ag(111) at +50 mV against SCE for $T = 296$, 302 and 307 K. The solid lines are fits to a $t^{1/2}$-law.

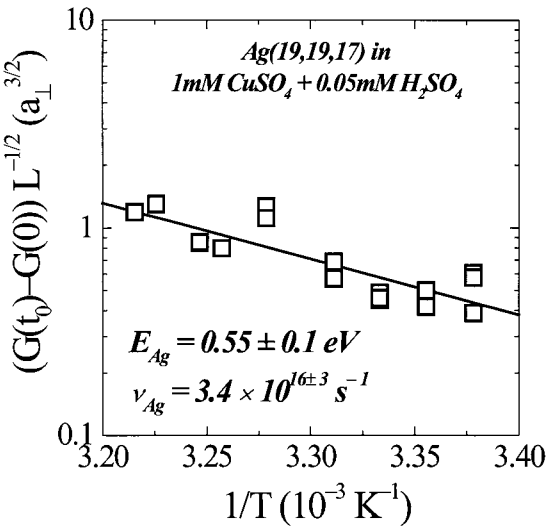

Figure 7. Arrhenius plot of the time correlation value $G(t_0)$ for $t_0 = 2$ s. To display data from different areas of the sample with different step densities in the same view graph, the data are scaled by the step–step distance L.

[26], who studied the decay of multilayer islands and found that the decay of islands is dominated by fast detachment of atoms from island edges and slow terrace diffusion. The slow surface diffusion compared to the last attachment/detachment kinetics at steps for Cu(111) in hydrochloric acid is most probably due to the presence of specifically absorbed chloride on the terraces which hinders the Cu surface diffusion due to site blocking.

For Cu(111) in UHV, edge diffusion is the dominant transport mechanism around room temperature and slow attachment kinetics with fast terrace diffusion prevails at temperatures

above 500 K [12]. In the temperature range between 285 and 315 K, $G(t_0)$ for $t_0 = 1$ s is between 0.1 and 0.3 $a_\perp^2$ in UHV. Comparing with figure 4 one finds that in HCl, $G(t_0)$ is almost two order of magnitudes larger than in UHV! In other words, specifically adsorbed chloride enhances the surface mobility on Cu(111), which was already previously discussed in the literature. Chloride is known to cause electrochemical annealing [51–54] of defects on metal electrodes, which decreases the metal electrode roughness. From our results we conclude that the surface diffusion is not only enhanced by two orders of magnitude but the dominant mass transport mechanism is considerably changed from edge diffusion in UHV to fast surface diffusion in HCl.

For comparison, we mention that we currently perform measurements of the step correlation function of Cu(111) in phosphoric acid [55]. Preliminary results show that $G(t)$ is proportional to $t^{1/4}$ around 300 K and the step fluctuations are about one order of magnitude larger than in UHV, however, still smaller than in HCl. We have not yet determined whether $G(t)$ depends on the step–step distance in phosphoric acid. Hence, we have yet no information on the dominant mass transport mechanism. It could be either edge diffusion (equation (10)) or terrace diffusion in presence of an Ehrlich–Schwoebel barrier.

To analyse the measured activation energy for Cu(111) (equation (20)), we rewrite the time law given in equation (15) where we have used $3E_{Cu} = 2\varepsilon + E_t$ and $t_0 = 1$ s:

$$\frac{G(t_0)}{a_\perp^2[s^{-1/3}]} \approx 1.72\, \nu_{Cu}^{1/3}\, \mathrm{e}^{-(2\varepsilon+E_t)/3k_BT}. \tag{24}$$

Hence, one finds with equation (20):

$$2\varepsilon + E_t = 0.84 \pm 0.12\ \mathrm{eV}. \tag{25}$$

As mentioned in section 3, equation (25) holds for any diffusing species since E_t is the activation energy of the chemical mass diffusion coefficient (equation (14)). If one assumes that the dominant mass diffusing species is one-atomic and low in concentration, equation (25) may be rewritten using $D_t = c_t D_t^{tr}$: the concentration of the diffusing species is $c_t = \mathrm{e}^{-E_{ad}/k_BT}$, with E_{ad} being its formation energy on the terrace. The tracer diffusion coefficient D_t^{tr} is set to $D_t^{tr} = \nu_{Cu}\, \mathrm{e}^{-E_{diff}/k_BT}$, with E_{diff} the surface diffusion barrier of the species. Hence, we find

$$2\varepsilon + E_{ad} + E_{diff} = 0.84 \pm 0.12\ \mathrm{eV}. \tag{26}$$

To the best of our knowledge, no experimental values for the individual energies are available for Cu(111) in electrolyte. One may compare equation (26) with experimental data available for Cu(111) in UHV: there, the kink formation energy at B-steps is 0.121 eV [46] and the sum of the adatom formation energy on the terrace and the diffusion barrier on the terrace is 0.76 eV [56]. From these values one obtains for the sum in the right-hand side of equation (26) about 1 eV, which is larger, however, of the same order of magnitude, as the energy found in electrolyte. From the fact that surface diffusion on Cu(111) in HCl is fast compared to the attachment/detachment at steps, whereas in UHV, surface diffusion is slow, we conclude that the results for the individual values of E_{ad} and E_{diff} may be considerably different from those in UHV, however.

5.2. Stepped Ag(111) in sulphuric acid

From equations (19) and (22) we find

$$\frac{G(t)}{L^{1/2}a_\perp^2[s^{-1/2}]} \approx 2\nu_{Ag}^{1/2}\, \mathrm{e}^{-(\varepsilon+E_{ad}+E_{sl})/2k_BT} \tag{27}$$

where we used $2E_{Ag} = \varepsilon + E_{ad} + E_{sl}$ and $t_0 = 2$ s. Furthermore, we have divided the left-hand side of equation (19) by $L^{1/2}$ to directly compare with the Arrhenius plot in figure 7.

The activation energy in equation (22) measured for $U = +50$ mV against the SCE can then be interpreted as

$$2E_{Ag}(50\text{ mV}) = 1.1 \pm 0.2\text{ eV} = \varepsilon(50\text{ mV}) + E_{ad}(50\text{ mV}) + E_{sl}(50\text{ mV}) \tag{28}$$

where the potential given in parentheses indicates that this equation holds for an electrode potential of +50 mV against the SCE.

As has been shown previously [27, 29], the kink formation energy ε for Ag(111) in 1 mM $CuSO_4$ + 0.05 mM H_2SO_4 is independent of the electrode potential in the range between −500 and +60 mV against the SCE and is determined as $\varepsilon \approx 0.1$ eV. Hence, we find

$$E_{ad}(50\text{ mV}) + E_{sl}(50\text{ mV}) = 1.0 \pm 0.2\text{ eV}. \tag{29}$$

For Ag(111), $G(t)$ depends strongly on the electrode potential, and hence, estimates for the activation energies may also be obtained from the data as shown in figure 5(b) [27, 29]: surface-embedded-atom calculations be Haftel and Einstein [57] show, that the potential dependence of mass transport energies on Ag(111) can be approximated by a linear function (at least for not too large potential ranges), hence

$$\begin{aligned} E_{ad}(U) &= E_{ad}(0) - \mathrm{e}\lambda_1 U \\ E_{sl}(U) &= E_{sl}(0) - \mathrm{e}\lambda_2 U. \end{aligned} \tag{30}$$

λ_1, λ_2 are the factors which define the linear relationship between the activation energies and the electrode potential. They must not be confused with the transfer coefficient. Using equation (30), equation (27) becomes (with $\lambda = \lambda_1 + \lambda_2$)

$$\frac{G(t)}{L^{1/2}a_\perp^2[s^{-1/2}]} \approx 2\nu_{Ag}^{1/2}\mathrm{e}^{(\mathrm{e}\lambda U/2k_BT)}\,\mathrm{e}^{-(\varepsilon+E_{ad}(0)+E_{sl}(0))/2k_BT} \tag{31}$$

which has an exponential dependence on the electrode potential U.

From the exponential fit to the previous [5] and our new data in figure 5(b), we find

$$\lambda = 1.43 \pm 0.28 \tag{32}$$

and (with $\varepsilon \approx 0.1$ eV [27, 29])

$$E_{ad}(0) + E_{sl}(0) = 1.0 \pm 0.2\text{ eV} \tag{33}$$

where we used $L = 81$ Å, $t = 2$ s and ν_{Ag} as given in equation (23). Here, the values in parentheses indicate that equation (33) holds for an electrode potential of 0 mV against the SCE. From equations (30), (32) and (33), we then calculate the corresponding results for an electrode potential of +50 mV against the SCE.

$$E_{ad}(50\text{ mV}) + E_{sl}(50\text{ mV}) = 0.9_3 \pm 0.2\text{ eV} \tag{34}$$

in excellent agreement with the direct result from the temperature dependent measurement given in equation (29). From UHV measurements of island decay on Ag(111) by Morgenstern *et al* [58] one finds that E_{ad} is of the order of 0.7 eV. Using this value in equation (34) one estimates the dissolution energy to be of the order of $E_{sl} \sim 0.2$ eV. Although this estimate is rather rough and E_{ad} may have a considerably different value in electrolyte, the small value for E_{sl} seems not be unreasonable. The data were obtained near the dissolution potential of silver where E_{sl} should vanish.

6. Summary

In this paper, it is demonstrated that quantitative data on diffusion barriers and activation energies of atomic mass transport may be obtained reproducibly by temperature variable STM studies of step motion on metal electrodes in electrochemical environment. Although the accessible temperature range for studies at the solid/liquid interface is small (compared, e.g. with similar investigations on metal surfaces in UHV), activation barriers may be determined with an error of about 10–20%. The reduction of the error bars is a matter of improvement of thermal drift stability of the STM set-up at least for systems in aqueous electrolytes. For metal electrodes in contact with non-aqueous electrolytes larger temperature ranges should be accessible and the determination may already been possible with a large accuracy. The application of temperature-variable STM to non-aqueous electrolytes, however, is left to future studies. We have further demonstrated that the presence of chloric acid in the electrolyte may not only enhance the surface mobility on metal electrodes but may also cause dramatic changes in the mass transport mechanism compared to UHV.

Acknowledgments

The authors are indebted to Udo Linke for his steady support with high quality metal electrodes for our studies. Furthermore, we acknowledge discussions with Harald Ibach and his critical reading of the manuscript. Financial support was delivered by the Fond der Chemischen Industrie.

References

[1] Giesen M 2001 *Prog. Surf. Sci.* at press
[2] Liu H, Fan F F, Lin C W and Bard A J 1986 *J. Am. Chem. Soc.* **108** 3838
[3] Sonnenfeld R and Hansma P K 1986 *Science* **232** 211
[4] Bartelt N C, Goldberg J L, Einstein T L and Williams E D 1992 *Surf. Sci.* **273** 252
[5] Bartelt N C, Einstein T L and Williams E D 1994 *Surf. Sci.* **312** 411
[6] Pimpinelli A, Villian J, Wolf D E, Métois J J, Heyraud J C, Elkinani I and Uimin G 1993 *Surf. Sci.* **295** 143
[7] Blagojevic B and Duxbury P M 1999 *Phys. Rev.* B **60** 1279
[8] Khare S V and Einstein T L 1998 *Phys. Rev.* B **57** 4782
[9] Bartelt N C, Goldberg J L, Einstein T L, Williams E D, Heyraud J C and Métois J J 1993 *Phys. Rev.* B **48** 15 453
[10] Pai W W, Bartelt N C and Reutt-Robey J E 1996 *Phys. Rev.* B **53** 15 991
[11] Giesen M, Icking-Konert G S, Stapel D and Ibach H 1996 *Surf. Sci.* **366** 229
[12] Giesen M and Icking-Konert G S 1998 *Surf. Sci.* **412–413** 645
[13] Giesen-Seibert M, Jentens R, Poensgen M and Ibach H 1993 *Phys. Rev. Lett.* **71** 3521
[14] Giesen-Seibert M and Ibach H 1994 *Surf. Sci.* **316** 205
[15] Giesen-Seibert M, Jentjens R, Poensgen M and Ibach H 1994 *Phys. Rev. Lett.* **73** E911
[16] Giesen-Seibert M, Schmitz F, Jentjens R and Ibach H 1995 *Surf. Sci.* **329** 47
[17] Kuipers L, Hoogeman M S and Frenken J W M 1993 *Phys. Rev. Lett.* **71** 3517
[18] Kuipers L, Hoogeman M S, Frenken J W M and v Beijeren H 1995 *Phys. Rev.* B **52** 11 387
[19] Hoogeman M S, Schlößer D C, Sanders J B, Kuipers L and Frenken J W M 1996 *Phys. Rev.* B **53** R13 299
[20] Hoogeman M S, Klik M A J, Schlößer D C, Kuipers L and Frenken J W M 1999 *Phys. Rev. Lett.* **82** 1728
[21] Speller S, Heiland W, Biedermann A, Platzgummer E, Nagl C, Schmid M and Varga P 1995 *Surf. Sci.* **331–333** 1056
[22] Barbier L, Masson L, Cousty J and Salanon B 1996 *Surf. Sci.* **345** 197
[23] Masson L, Barbier L and Cousty J 1994 *Surf. Sci.* **317** L1115
[24] Masson L, Barbier L, Cousty J and Salanon B 1994 *Surf. Sci.* **324** L378
[25] Dakkouri A S, Randler R and Kolb D M 1997 *Proc. Symp. on the Electrochemical Double Layer* vol 97-17, ed C Kozeniewski and B E Conway (Pennington, NJ: Electrochemical Society)
[26] Broekmann P, Wilms M, Kruft M, Stuhlmann C and Wandelt K 1999 *J. Electroanal. Chem.* **467** 307

[27] Giesen M, Dietterle M, Stapel D, Ibach H and Kolb D M 1997 *Surf. Sci.* **384** 168
[28] Giesen M, Dietterle M, Stapel D, Ibach H and Kolb D M 1997 *Electrochemical Synthesis and Modification of Materials* vol 451, ed P C Andricacos *et al* (Pittsburgh, PA: Material Research Society) p 9
[29] Giesen M, Randler R, Baier S, Ibach H and Kolb D M 1999 *Electrochim. Acta* **45** 533
[30] Baier S and Giesen M 2000 *Phys. Chem. Chem. Phys.* **2** 3675
[31] McHardy R, Haiss W H and Nichols R J 2000 *Phys. Chem. Chem. Phys.* **2** 1439
[32] Giesen M and Kolb D M 2000 *Surf. Sci.* **468** 149
[33] Bach C E, Nichols R J, Beckmann W, Meyer H, Schulte A, Besenhard J O and Jannakoudakis P D 1993 *J. Electrochem. Soc.* **140** 2181
[34] Wintterlin J, Schuster R, Coulman D J, Ertl G and Behm R J 1990 *J. Vac. Sci. Technol.* B **9** 902
[35] Wolf J F, Vicenzi B and Ibach H 1991 *Surf. Sci.* **249** 233
[36] Poensgen M, Wolf J F, Frohn J, Giesen M and Ibach H 1992 *Surf. Sci.* **274** 430
[37] Kitamura N, Lagally M G and Webb M B 1993 *Phys. Rev. Lett.* **71** 2082
[38] Dietterle M, Will T and Kolb D M 1995 *Surf. Sci.* **327** L495
[39] Moffat T P 1997 *Electrochemical Synthesis and Modification of Materials* vol 451, ed P C Andricacos *et al* (Pittsburgh, PA: Materials Research Society) p 75
[40] Bartelt N C, Einstein T L and Williams E D 1990 *Surf. Sci.* **240** L591
[41] Williams E D, Phaneuf R J, Wei J, Bartelt N C and Einstein T L 1993 *Surf. Sci.* **294** 219
[42] Williams E D, Phaneuf R J, Wei J, Bartelt N C and Einstein T L 1994 *Surf. Sci.* **310** 451
[43] Einstein T L 1999 private communication
[44] Dieluweit S, Giesen M, Ibach H and Krug J 2001 to be published
[45] Nozières P 1991 *Solids Far From Equilibrium* ed C Godrèche (Cambridge: Cambridge University Press) p 1
[46] Steimer C, Giesen M and Ibach H 2001 *Surf. Sci.* **471** 80
[47] Ehrlich G and Hudda F G 1966 *J. Chem. Phys.* **44** 1039
[48] Schwoebel R L and Shipsey E J 1966 *J. Appl. Phys.* **37** 3682
[49] Wilms M, Broekmann P, Stuhlmann C and Wandelt K 1998 *Surf. Sci.* **416** 121
[50] Kellogg G L 1994 *Surf. Sci. Rep.* **21** 1
[51] Cali G J, Berry G M, Bothwell M E and Soriaga M P 1991 *J. Electroanal. Chem.* **297** 523
[52] Dakkouri A S 1997 *Solid State Ion.* **94** 99
[53] Goetting L B, Huang B M, Lister T E and Stickney J L 1995 *Electrochim. Acta* **40** 143
[54] Stickney J L, Villegas I and Ehlers C B 1989 *J. Am. Chem. Soc.* **111** 6473
[55] Dieluweit S and Giesen M 2001 to be published
[56] Icking-Konert G S, Giesen M and Ibach H 1998 *Surf. Sci.* **398** 37
[57] Haftel M I and Einstein T L 2000 *Nucleation and Growth Processes in Materials* vol 580, ed A Gonis, P E A Turchi and A J Ardell (Pittsburgh, PA: Materials Research Society) p 195
[58] Morgenstern K, Rosenfeld G and Comsa G 1996 *Phys. Rev. Lett.* **76** 2113